ES Materials and Manufacturing
DOI: https://dx.doi.org/10.30919/esmm969

La_2CuO_4 Electrode Material For Low Temperature Solid Oxide Fuel Cells

Mazhyn K. Skakov[1, 2,*] Sana K. Kabdrakhmanova,[2, 3,*] Kydyrmolla Akatan,[2,*] Almira M. Zhilkashinova,[2] Esbol Shaimardan,[4] Madiyar M. Beisebekov,[4] Kantai Nurgamit,[2] Viktor V. Baklanov,[5] Yerbolat T. Koyanbayev,[5] Arman Zh Miniyazov,[5] Igor A. Sokolov[5] and Nurya M. Mukhamedova[5]

Abstract

Presently, scientists are vigorously exploring effective, sustainable and environmentally friendly energy sources, which has lent momentum to the adoption of solid oxide fuel cells (SOFCs). The present research focuses on the synthesis and investigation of a binary oxide composed of lanthanum and copper, which was characterized using FTIR, XRD, SEM, XPS and BET. The findings revealed that the surface morphology exhibited mesoporosity, due to the interconnection and sintering of the pliable, rod-like crystalline structure, which was determined to be the binary oxide La_2CuO_4. Furthermore, within the temperature range of 500 to 600 °C, a two-fold increase in current density through the anode material was observed for every 50 °C temperature increment, coupled with a nearly three-fold reduction in polarized resistance.

Keywords: Binary oxide; Anode materials; Solid oxide fuel cells; La_2CuO_4; Copper-based anode.
Received: 18 September 2023; Revised: 27 September 2023; Accepted: 30 September 2023.
Article type: Research article.

1. Introduction

Promoting technologies that balance environmental sustainability with effective energy utilization stands as a paramount goal in contemporary scientific pursuits, allowing the rapid adoption of new technologies, such as solid oxide fuel cells (SOFCs). In comparison to other fuel cell varieties, SOFCs are distinguished by their extended operational lifespan, as well as impressive efficiency, reaching approximately 60%.[1] A notable advantage lies in the versatility of fuel sources, which extends beyond hydrogen to encompass natural gas, biogas and propane. Additionally, the environmental footprint of SOFC technology is remarkably reduced in contrast to conventional electricity generation methods, resulting in minimal waste emissions.[2] Furthermore, a possibility exists to harness the heat created through cogeneration.[3]

Nonetheless, the elevated temperature within the SOFC membrane-electrode unit (MEA) diminishes the system's operational lifespan, lowers the efficiency of the catalyst, and triggers thermal expansion-induced diffusion between the electrolyte and electrodes.[4] Moreover, the production of specialized cathode, anode and heat-resistant membrane materials, along with the necessity for ongoing maintenance and repair, become imperative.[5]

The energy power density in an SOFC is chiefly determined by the surface area and materials used in the cathode, anode and electrolytes.[6] Consequently, this poses challenges when designing economically affordable and portable SOFCs.[7] Therefore, the primary research focus has revolved around enhancing the composition of ceramic oxides utilized in fabricating electrode materials and membranes, while concurrently lowering operating temperatures.[8]

Currently, the anode material most commonly employed in SOFCs is yttrium-stabilized zirconia (YSZ), along with a nickel-based catalyst. However, following the introduction of small amounts of additives, the nickel is adulterated, quickly decreasing its catalytic activity.[9] A review of the literature shows that ceramic materials derived from copper and rare earth elements hold substantial promise in addressing these

[1] *National Nuclear Center of the Republic of Kazakhstan, Kurchatov, 071100, Kazakhstan.*
[2] *National scientific laboratory, S. Amanzholov East Kazakhstan University, Oskemen, 070020, Kazakhstan.*
[3] *Department of Chemical and Biochemical Engineering, Satbayev University, Almaty, 050000, Kazakhstan.*
[4] *Scientific Center of Composite Materials, Almaty, 050000, Kazakhstan.*
[5] *Institute of Atomic Energy, branch of the National Nuclear Center of the Republic of Kazakhstan, Kurchatov, 071100, Kazakhstan.*
**Email:* sanaly33@mail.ru (S. K. Kabdrakhmanova), ahnur.hj@mail.ru (A. Kydyrmolla)

issues.[1,10-13] Some studies have demonstrated that a Cu-Ce anode possesses excellent conductivity and remarkable resistance to damage, particularly within the tubular and planar cells. In such a setup, the copper primarily serves as the conduit for the current, while the cerium exhibits notable catalytic activity in oxidation reactions. Moreover, the Cu-Ce anode material has been investigated for its ability to withstand corrosion induced by sulfur and redox reactions.[10,14] Therefore, incorporating copper, which boasts catalytic activity comparable to nickel, in the fabrication of anode materials has a beneficial impact on lowering the operating temperature of the electrode-membrane unit and extending the longevity of the catalytic system.[11,15]

During a particular study, an anode material based on cerium doped with 35-45% Cu-Li-Gd was synthesized at a temperature of 900-950 °C, and its electrochemical characteristics were then studied at a temperature of 600 °C. Nevertheless, operational tests revealed a migration of copper towards the electrolyte, which raises concerns about potential reductions in the operational lifespan of such a cell. In a related study,[10] an anode comprising 10 layers, constructed from cerium doped with copper and gadolinium was manufactured. At a temperature of 650 °C, the maximum output power was observed to reach 225 mV/cm^2, and the energy output was shown to demonstrate a dependency on the number of layers. This underscores the substantial promise of composites utilizing copper and rare earth elements in anode material formulation.

During the present study, an anode material based on Cu-La was synthesized for use in SOFCs, following which its physical, chemical and morphological characteristics were analyzed, and its electrical properties were then studied over a temperature range of 500-600 °C.

2 Materials and methods

2.1 Chemicals and materials

Lanthanum (III) nitrate hexahydrate ($La(NO_3)_3 \cdot 6H_2O$ 99.99%), *copper(II) sulfate pentahydrate* ($CuSO_4 \cdot 5H_2O$, *98.0%)*, and acrylamide (*C_3H_5NO, 99%) were purchased from Sigma-Aldrich (India)*. The original $La(NO_3)_3 \cdot 6H_2O$ and $CuSO_4 \cdot 5H_2O$ were pre-dried in a vacuum oven (LabSol, China) for 2 hours at a temperature of 110°C, in order to remove any water adsorbed and carbon dioxide. All reagents were used as is, without preliminary purification.

2.2 Synthesis of binary oxide

0.5 g of $La(NO_3)_3 \cdot 6H_2O$ and 0.5 g of $CuSO_4 \cdot 5H_2O$ were combined with 1 g of acrylamide, then thoroughly ground using an agate mortar until a smooth consistency was achieved. The mixture obtained was transferred to a porcelain crucible and stirred vigorously with a glass rod for 30 minutes until black cotton consistency was achieved, while adding 25 ml of deionized water. Subsequently, the solution underwent calcination in an electric furnace at a temperature of 200 °C. The resulting black cotton mass was subjected to thermal activation in a Fibre Muffle 1100 furnace (SNOL, Lithuania) for 1 hour at a temperature of 800±10 °C. The mass obtained was cooled and ground in a Pulverisette-6 planetary ball mill (FRITSCH, Germany) for 15 min at 300 rpm. As a result, the particle size of the resulting powder was 10±1 μm, at a yield of 43±3%.

2.3 FTIR analysis

FTIR analysis of the La_2CuO_4 was performed using an FT-801 FTIR spectrometer (Simex, Russia), with a resolution of 1 cm^{-1} at a range of 300-4700 cm^{-1}, at a temperature of 25±10 ºC, in accordance with the standard method. An accessory was used to measure attenuated total reflection (ATR) and specular-diffuse reflection (SDR).

2.4 XRD analysis

The crystal structure of the resulting La_2CuO_4 was studied utilizing X-ray diffraction on an X´Pert PRO diffractometer (Malvern Panalytical, Netherlands), using monochromatized copper (CuKα) radiation at a scanning speed of 0.05º for 10 s, with a K-Alpha1 wavelength 1.54187 Å. Reflection mode measurements using a rectangular aluminum universal sample holder (PW1172/01) were carried out at a 2θ diffraction angle of 10° to 80°, with X-ray tube voltage of 45 kV and current of 30 mA., with a measurement time of each step at 0.5 s. The ICDD PDF-4/AXIOM radiograph database was used to analyze the radiographs obtained, and the POWDER CELL 2.5 software package was utilized in refining the Rietveld unit cell parameters.

2.5 SEM analysis

The microstructure of La_2CuO_4 was analyzed using a Quanta 3D 200i SEM (FEI, Netherlands), with measurements carried out in high vacuum mode utilizing a secondary electron detector at an accelerating voltage of 5 kV. In order to obtain the EDX spectrum, the accelerating voltage was set to 15 kV.

2.6 Adsorption porosimetry

The textural properties of La_2CuO_4 were evaluated employing adsorption porosimetry, specifically low-temperature nitrogen adsorption, using an Autosorb 1 surface area and porosity analyzer (Quantachrome Instruments, USA) and an ASAP-2020 adsorption analyzer (Micromeritics, USA). Prior to analysis, the samples underwent vacuum degassing for 20 hours at a temperature range of 200 to 220 °C. The experimental data were subsequently assessed using the Brunauer-Emmett-Teller (BET) and Barrett-Joyner-Halenda (BJH) methods. For the determination of the volume (V) to pressure (P) relationship at a constant temperature, which is the adsorption isotherm, the adsorbent sample was degassed under vacuum conditions at temperatures within the range of 200-300 °C. The specific surface area was quantified using the BET method, with an associated measurement error (Δ) of ±2.8 rel.%, using the above apparati. In order to ascertain the distribution of both total volume and pore size, the BJH

method was applied, utilizing desorption isotherm data.

2.7 XPS analysis

XPS spectra (Thermo Fisher Scientific, USA) were obtained using a NEXSA X-Ray photoelectron spectrometer, with pass energy of 50 eV for the survey scan and 20 eV for individual scans, at 380 W operating power. The XPS positions were referenced using the Carbon (1s) peak at 284.5 eV. Prior to actual analysis, the samples were pre-treated in a desorption chamber, maintained at 10^{-9} Torr vacuum.

2.8 Electrical characteristics

Galvanostatic assessments were conducted at a fixed current density of 0.44 A/cm^{-2}. Electrochemical impedance spectroscopy (EIS) was performed using an CS model potentiostat/galvanostat (Corrtest, China). The EIS measurements were performed under open-circuit conditions across a frequency spectrum spanning from 0.1 Hz to 5 kHz, utilizing a signal amplitude of 10 mV. The investigations were conducted at temperatures of 500 °C, 550 °C, and 600 °C. In order to prepare the sample for the study, La_2CuO_4 was blended with terpineol to produce a gel-like suspension. This resultant gel was subsequently applied onto a Ni foam plate at a pressure of 250 MPa, followed by drying at a temperature of 120±10 °C for a duration of 2 hours. The prepared anode material was then cut into a symmetrical configuration with a thickness of 2 mm and a surface area of 0.64 cm^2.

3. Results and discussion

3.1 FTIR analysis

The chemical structure of the La_2CuO_4 binary oxide was studied using FTIR (Fig. 1a). The samples show bands at 490, 596, 649 and 1420 cm^{-1}, assigned to the stretching mode of Cu–O and La–O–H groups.[16] The low intensity bands observed at 502, 1065 and 591, 1108 cm^{-1} correlate to the Cu–O and La–O stretching modes of orthorhombic La_2CuO_4 phase. Further, the presence of bands at 596 and 1187 cm^{-1}, related to the Cu–O stretching mode, in all the samples confirm the presence of Cu–O as the secondary phase, the reason for which is the 1:1 precursor ratio and the product formed with a A_2BO_4-type structure.[17] The obtained La_2CuO_4 through a hydrothermal treatment of a mixture of copper and lanthanum nitrates for 6 hours, followed by calcination at 900 °C. However, in this study, the synthesis process only took 1.5 hours.

3.2 XRD analysis

The X-ray diffraction pattern of the La_2CuO_4 binary oxide is shown in Fig. 1b. Following temperature treatment of the oxide composition at 800 °C, the Miller indices were found to be 24.58° (111), 27.03° (131), 31.06°(002), 33.17° (200), 41.11° (060), 41.67° (151), (200), 43.41° (042), 44.74° (061), 47.77° (202), 53.94° (113), 55.78° (080), 58.23° (331), 64.91° (153), 66.56° (082), 70.19° (400), 75.23° (371), 76 49° (282) and 78.37° (083), demonstrating that the orthorhombic crystal based on the binary oxide La_2CuO_4 consists of a lattice phase. Some studies have established that during the synthesis of carbamate derivatives of lanthanum and copper using the $NHBu_2/CO_2$ reaction, a phase corresponding to the orthorhombic crystal lattice of La_2CuO_4 is formed, after which the resulting precipitate is treated at a temperature of 800 °C.[1,2] Such results are consistent with those obtained in the present study.

3.3 SEM analysis

The results of SEM analysis of the binary oxide La_2CuO_4 are shown in Figs. 2a-d. The surface morphology of the La_2CuO_4 can be seen to be agglomerated and to contain large porous particles (Fig. 2a). The morphology of La_2CuO_4 becomes porous due to the presence of carbon dioxide and evaporating water released during the formation of the complex oxide through primary homogenization and heating at 200 °C (Figs. 2b, 2c). At a high temperature (800 °C), the porous morphology of the La_2CuO_4 changes into an agglomeration of rod-shaped structures (Fig. 2d).[18] Such rods were found to have a length of 171.6-209.0 nm and a diameter of 65.03-75.43 nm. The sizes of pores formed during mutual adhesion of the rods were discovered to range from 314.4 nm down to 1.338 µm. A similar morphological structure was identified in previous research.[18,19] The EDS result showed that the elements La and Cu constitute the matrix of the binary oxide La_2CuO_4 (Fig. 3).

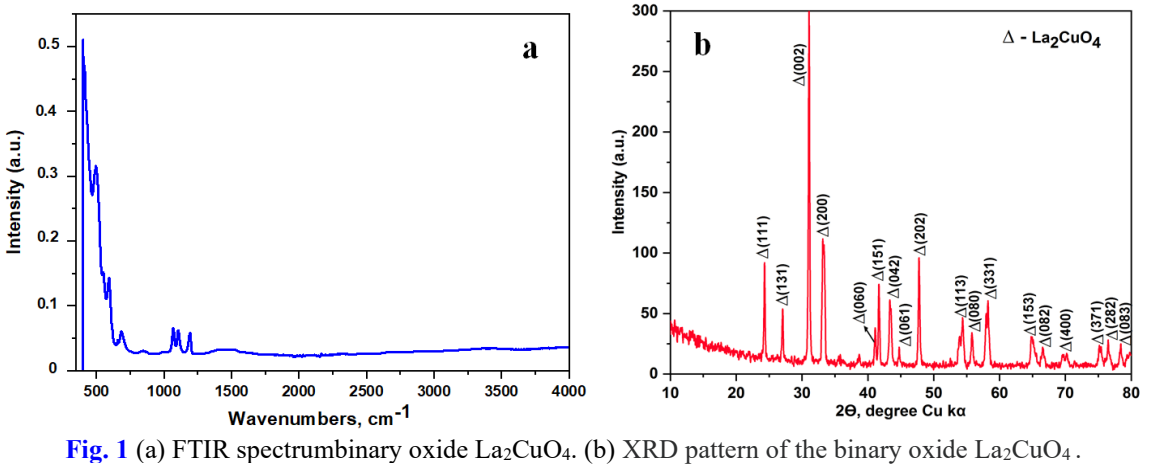

Fig. 1 (a) FTIR spectrumbinary oxide La_2CuO_4. (b) XRD pattern of the binary oxide La_2CuO_4 .

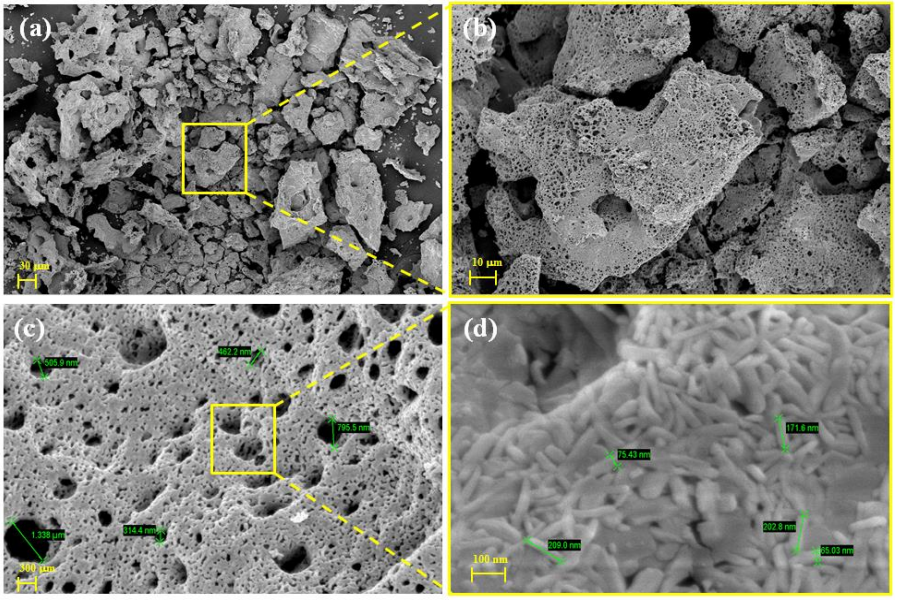

Fig. 2 SEM images of the binary oxide La_2CuO_4.

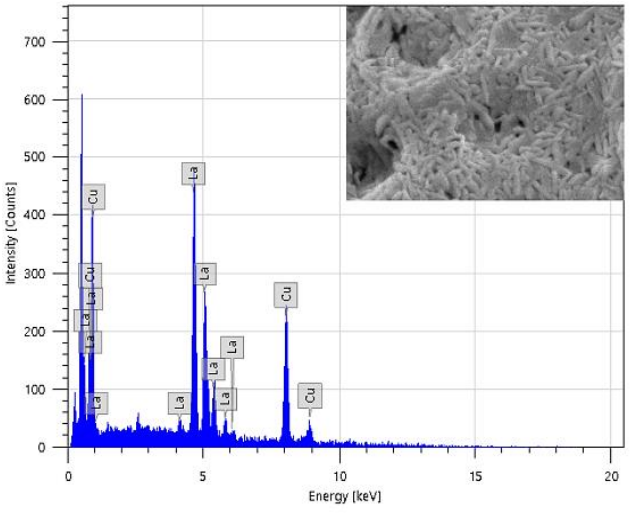

Fig. 3 The EDS mapping analysis of the binary oxide La_2CuO_4.

3.4 Adsorption porosimetry

The nitrogen adsorption-desorption isotherms of the La_2CuO_4 binary oxide are shown in Fig. 4a. The curve is indicative of a type IV nitrogen adsorption isotherm, and confirms the material as being mesoporous. La_2CuO_4 was shown to exhibit H1-type hysteresis due to the cylindrical channels.[20] The results indicate a blocking effect of the material in the process of nitrogen sorption, an effect which, accordingly, applies to large porous structures in alloyed metals.[21] Based on the nitrogen adsorption isotherm, La_2CuO_4 demonstrated monolayer adsorption on the walls of the mesopores at relative pressure (P/P0) ranging from 0 to 0.8. Further, the calculated surface area of La_2CuO_4 was 123.87 m^2/g, with an average pore radius of ≈ 14.25 nm (Fig. 4b). The variation in pore radius values is attributed to the influence of carbon dioxide and evaporated water during synthesis. We see that this is consistent with the SEM result (Fig. 2). It was determined that the surface area of the synthesized $CuCeO_2$ binary oxide is equal to 31.9 m^2/g. The surface area of the La_2CuO_4 binary oxide obtained in this study was 3.9 times greater.

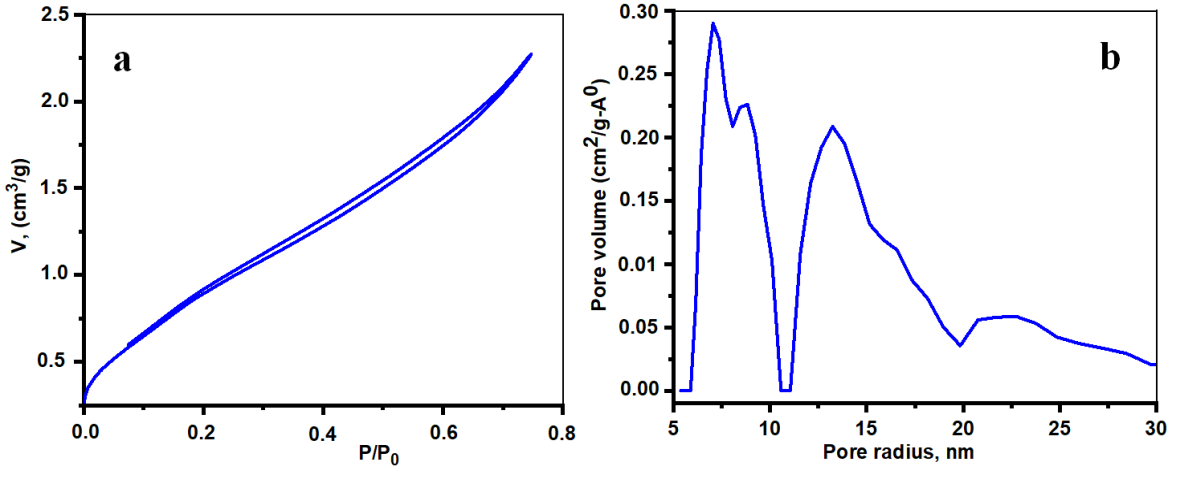

Fig. 4 (a) Nitrogen adsorption-desorption isotherms of the binary oxide La_2CuO_4. (b) Pore size distribution of the binary oxide La_2CuO_4.

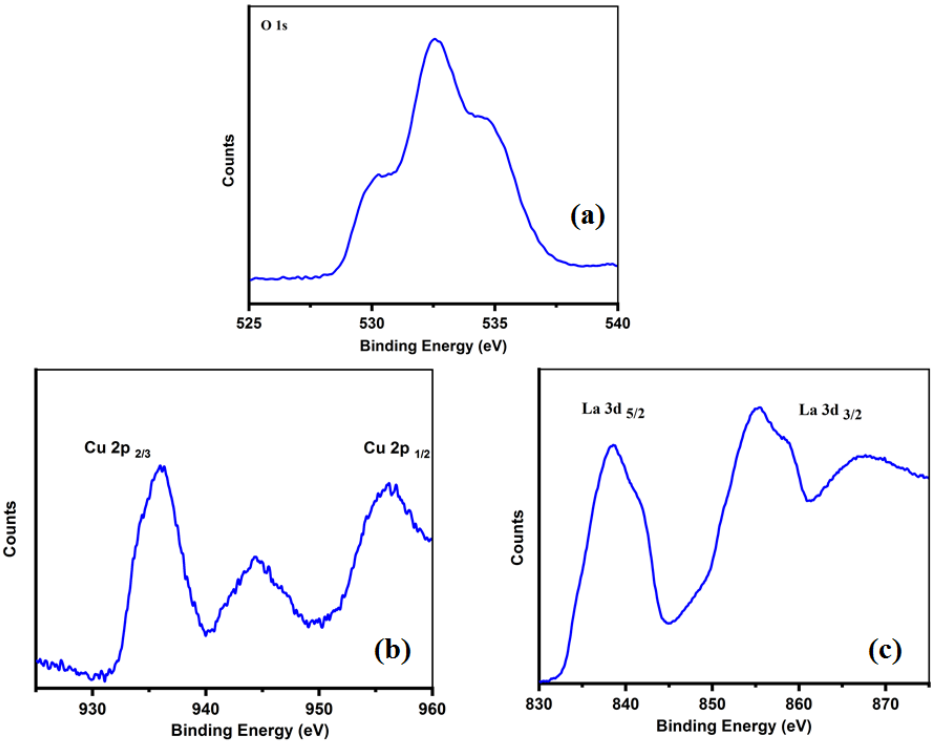

Fig. 5 XPS spectra of the binary oxide La_2CuO_4.

3.5 X-ray Photoelectron spectroscopy (XPS)

Photoelectron spectroscopy (XPS) revealed peaks in the O1s, $Cu_2p_{3/2}$, $Cu_2p_{1/2}$ and $La_3d_{5/2}$, $La_3d_{3/2}$ regions (Fig. 5). In the O1s region, a high, irregular Gaussian peak is seen, along with minor assymetrically located plateaus on either side, which shows a binding energy (BE) of 532.5 eV (Fig. 5a). The regions of $Cu_2p_{3/2}$ and $Cu_2p_{1/2}$ were observed at a BE value of 935.4 eV, with a characteristic satellite structure in the BE region of 945–955 eV. The ratio of the intensity of the satellite line to that of the $Cu_2p_{3/2}$ region is about 0.25 (with a corresponding value for CuO at 0.55), which is very close to that obtained in many superconducting copper oxide compounds[22] (Fig. 5b). The BE value of $Cu_2p_{3/2}$ in La_2CuO_4 is between those observed for CuO (933.4) and Cu_2O (934.6). The $La_3d_{5/2}$ region shows a pronounced asymmetry on the low binding energy side (Fig. 5c). The La_3d level, along with its satellite structure, resolved into multiple Gaussian peaks. The first pair had a value of BE 837.7 (Lai), whereas the second pair had BE values of 853.6 (Lall). The BE values of the first pair are very close to the La values of La_2O_3, and the BE values of the second pair are very close to both $La(OH)_3$ and $La_2(CO_3)_3$. Thus, the results obtained are in good agreement with previous studies.[22-24]

3.6 Electrical characteristics

We determined the electrochemical characteristics of the

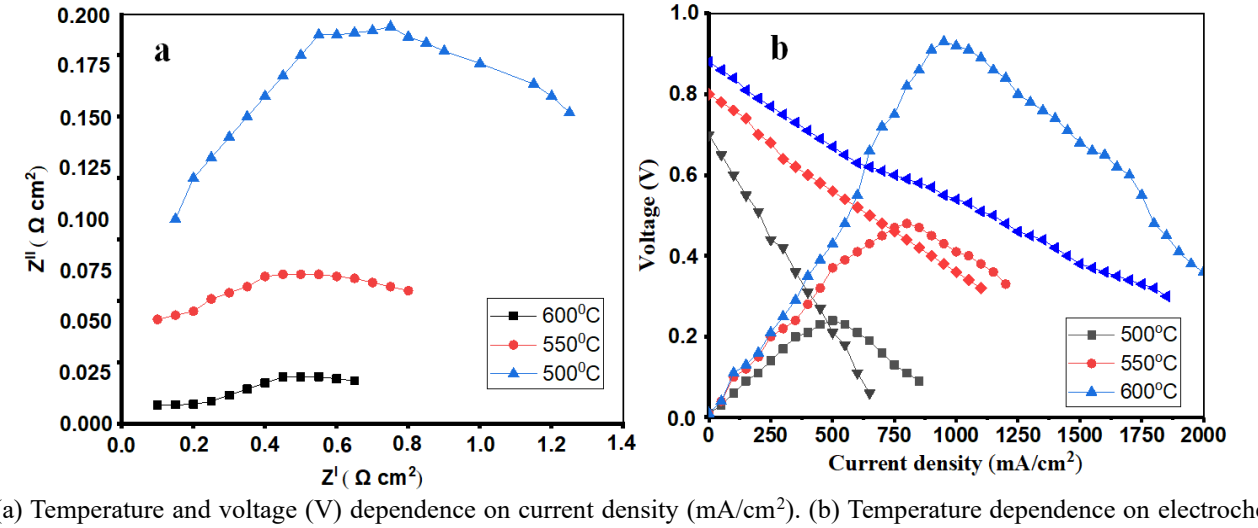

Fig. 6 (a) Temperature and voltage (V) dependence on current density (mA/cm^2). (b) Temperature dependence on electrochemical impedance.

La_2CuO_4 anode material within a relatively low temperature range. Fig. 6a shows the I-P curves of a mixture of 1.5% water and bubble of hydrogen with the La_2CuO_4 anode material over a temperature range of 500 °C-600 °C. The peak densities were 0.23 W/cm^{-2} at 500 °C, 0.48 W/cm^{-2} at 550 °C, and 1.05 W/cm^{-2} at 600 °C. Comparing the numerical values obtained at the various temperatures, the current density through the anode material is clearly shown to rise by two times with each temperature increase of 50°C. The temperature dependence of the La_2CuO_4 anode material anode was found to be similar to that based on La-Ni.[25]

Figure 6b shows the electrochemical impedance curves of a mixture of 1.5% water and bubble of hydrogen with the La_2CuO_4 anode material over a temperature range of 500 °C-600 °C. Note that the numerical values obtained showing polarization resistance decrease as temperature increases (Table 1). The polarized resistance of the La_2CuO_4 anode material was demonstrated to decrease by approximately three times with each temperature increase of 50 °C, which means that when the anode material is in contact with hydrogen, the La-Cu present shows an active catalytic property in the decomposition of hydrogen.[26] Similar results were obtained in a similar study using anode material consisting of the complex oxides of Cu-$Ce_{0.8}Sm_{0.2}O_{2-\delta}$. When compared, the electrochemical characteristics of the anodic system consisting of binary oxides (La_2CuO_4) utilized in the present study were found not to be inferior to other complex oxide systems.

Table 1. Quantitative values of the polarization resistance of the anode material over the temperature range of 500-600 °C.

Anode material	500 °C	550 °C	600 °C
La_2CuO_4	0.19 Ω·cm^2	0.07 Ω·cm^2	0.02 Ω·cm^2

4. Conclusion

The binary oxide La_2CuO_4 was synthesized using the sol-gel method. Following characterization with FTIR, XRD, SEM, XPS and BET, the electrical characteristics of the La_2CuO_4 anode material were examined. In a 1.5% mixture of water and bubble of hydrogen, the current density passing through the anode material was discovered to increase by two times, and the polarized resistance to decrease by approximately three times, for every 50°C rise over a temperature range of 500-600°C. The results obtained showed that the La_2CuO_4 composite oxide is a reasonable option for use as an anode material for SOFCs. The present research team plans to perform further experiments in order to compare the effectiveness of La_2CuO_4 against both existing and proposed complex and binary oxides, so as to find the lowest cost materials that provide the best characteristics for the production of electrodes to be used in SOFCs.

Acknowledgments

This research has been funded by the Science Committee of the Ministry of Science and Higher Education of the Republic of Kazakhstan (Grant No. BR10965284).

Conflict of Interest

There is no conflict of interest.

Supporting Information

Not applicable.

References

[1] M. Singh, D. Zappa, E. Comini, Solid oxide fuel cell: decade of progress, future perspectives and challenges, *International Journal of Hydrogen Energy*, 2021, **46**, 27643-27674, doi: 10.1016/j.ijhydene.2021.06.020.

[2] N. Mahato, A. Banerjee, A. Gupta, S. Omar, K. Balani, Progress in material selection for solid oxide fuel cell technology: a review, *Progress in Materials Science*, 2015, **72**, 141-337, doi: 10.1016/j.pmatsci.2015.01.001.

[3] S. Zarabi Golkhatmi, M. I. Asghar, P. D. Lund, A review on solid oxide fuel cell durability: latest progress, mechanisms, and study tools, *Renewable and Sustainable Energy Reviews*, 2022, **161**, 112339, doi: 10.1016/j.rser.2022.112339.

[4] V. De Marco, A. Iannaci, S. Rashid, V. M. Sglavo, Performance and evolution of planar copper-based anode-supported solid oxide fuel cells, *Journal of the Ceramic Society of Japan*, 2017, **125**, 313-316, doi: 10.2109/jcersj2.16243.

[5] I. Sreedhar, B. Agarwal, P. Goyal, S. A. Singh, Recent advances in material and performance aspects of solid oxide fuel cells, *Journal of Electroanalytical Chemistry*, 2019, **848**, 113315, doi: 10.1016/j.jelechem.2019.113315.

[6] M. Bianco, P. Caliandro, S. Diethelm, S. Yang, A. Dellai, J. Van herle, R. Steinberger-Wilckens, *In-situ* experimental benchmarking of solid oxide fuel cell metal interconnect solutions, *Journal of Power Sources*, 2020, **461**, 228163, doi: 10.1016/j.jpowsour.2020.228163.

[7] Y. Pan, S. Geng, G. Chen, F. Wang, $CuFe_2O_4$/CuO coating for solid oxide fuel cell steel interconnects, *International Journal of Hydrogen Energy*, 2021, **46**, 22942-22955, doi: 10.1016/j.ijhydene.2021.04.117.

[8] V. De Marco, A. Iannaci, S. Rashid, V. M. Sglavo, Performance and evolution of planar copper-based anode-supported solid oxide fuel cells, *Journal of the Ceramic Society of Japan*, 2017, **125**, 313-316, doi: 10.2109/jcersj2.16243.

[9] D. Papurello, A. Lanzini, S. Fiorilli, F. Smeacetto, R. Singh, M. Santarelli, Sulfur poisoning in Ni-anode solid oxide fuel cells (SOFCs): Deactivation in single cells and a stack, *Chemical Engineering Journal*, 2016, **283**, 1224-1233, doi: 10.1016/j.cej.2015.08.091.

[10] F. Zurlo, A. Iannaci, V. M. Sglavo, E. Di Bartolomeo, Copper-based electrodes for IT-SOFC, *Journal of the European Ceramic Society*, 2019, **39**, 17-20, doi: 10.1016/j.jeurceramsoc.2018.02.029.

[11] V. De Marco, A. Grazioli, V. M. Sglavo, Production of planar copper-based anode supported intermediate temperature solid oxide fuel cells cosintered at 950 °C, *Journal of Power Sources*, 2016, **328**, 235-240, doi: 10.1016/j.jpowsour.2016.08.025.

[12] K. Binnemans, P. T. Jones, B. Blanpain, T. Van Gerven, Y. Yang, A. Walton, M. Buchert, Recycling of rare earths: a critical review, *Journal of cleaner production*, 2013, **51**, 1-22, doi: 10.1016/j.jclepro.2012.12.037.
[13] V. De Marco, A. Grazioli and V. M. Sglavo, Production and co-sintering at 950 °C of planar half cells with CuO-GDC cermet supporting anode and Li_2O-Doped GDC electrolyte, *Ceramic Engineering and Science Proceedings*, 2016, **37**, 31-38, doi: 10.1002/9781119320197.ch3
[14] S. Jung, C. Lu, H. He, K. Ahn, R. J. Gorte, J. M. Vohs, Influence of composition and Cu impregnation method on the performance of Cu/CeO_2/YSZ SOFC anodes, *Journal of Power Sources*, 2006, **154**, 42-50, doi: 10.1016/j.jpowsour.2005.04.018.
[15] V. Dipti, Dharmadhikari, Template free hydrothermal synthesis and gas sensing application of lanthanum cuprate (La_2CuO_4): effect of precursors on phase formation and morphology, *Journal of Alloys and Compounds*, 2014, **590**, 486-493, doi: 10.1016/j.jallcom.2013.12.141.
[16] Y. Su, L. Dai, Q. Zhang, Y. Li, J. Peng, R. Wu, W. Han, Z. Tang, Y. Wang, Fabrication of Cu-doped CeO_2 catalysts with different dimension pore structures for CO catalytic oxidation, *Catalysis Surveys from Asia*, 2016, **20**, 231-240, doi: 10.1007/s10563-016-9220-z.
[17] A. Rahmani, J. Saffari, Preparation, structure and selected catalytic properties of La_2CuO_4 nano mixed metal oxides, *Journal of Nanostructures*, 2016, **6**, 301-306, doi: 10.22052/JNS.2016.34270.
[18] Huihuang, Jiang, Preparation, characterization and electrochemical properties of La_2CuO_4@Au as a novel bifunctional oxygen electrode, *International Journal of Electrochemical Science*, 2020, **15**, 9933-9939, doi: 10.20964/2020.10.74.
[19] J. Wang, C. Cheng, B. Huang, J. Cao, L. Li, Q. Shao, L. Zhang, X. Huang, Grain-boundary-engineered La_2CuO_4 perovskite nanobamboos for efficient CO_2 reduction reaction, *Nano Letters*, 2021, **21**, 980-987, doi: 10.1021/acs.nanolett.0c04004.
[20] Z. Razmara, Sonochemical synthesis, thermal behavior and luminescent properties of copper(II) supramolecular, a precursor for preparation of CuO nanoparticles and the study of their photocatalytic activity, *Journal of Inorganic and Organometallic Polymers and Materials*, 2018, **28**, 2407-2417, doi: 10.1007/s10904-018-0906-8.
[21] D. Zhang, D. Wei, Z. Cui, S. Wang, S. Yang, M. Cao, C. Hu, Improving water splitting performance of Cu_2O through a synergistic "two-way transfer" process of Cu and graphene, *Phys Chem Chem Phys*, 2014, **16**, 25531-25536, doi: 10.1039/c4cp02904f.
[22] S. Badrinarayanan, A. B. Mandale, S. R. Sainkar, N. R. Pavaskar, V. Ramaswamy, The stability of the surface of La_2CuO_4 to reactions with adsorbed n-butyl amine: X-ray photoelectron spectroscopy study, *Journal of Materials Research*, 1994, **9**, 1140-1146, doi: 10.1557/JMR.1994.1140.
[23] K. H. Lee, R. Hoffmann, Oxygen interstitials in superconducting La_2CuO_4: their valence state and role, *The Journal of Physical Chemistry A*, 2006, **110**, 609-617, doi: 10.1021/jp053154f.
[24] M. Velasquez, A. Santamaria, C. Batiot-Dupeyrat, Selective conversion of glycerol to hydroxyacetone in gas phase over La_2CuO_4 catalyst, *Applied Catalysis B: Environmental*, 2014, **160-161**, 606-613, doi: 10.1016/j.apcatb.2014.06.006.
[25] A. Yan, M. Phongaksorn, D. Nativel, E. Croiset, Lanthanum promoted NiO-SDC anode for low temperature solid oxide fuel cells fueled with methane, *Journal of Power Sources*, 2012, **210**, 374-380, doi: 10.1016/j.jpowsour.2011.10.081.
[26] Y. Zhang, Z. Huang, T. Gan, N. Hou, L. Fan, X. Zhou, G. Gao, J. Li, Y. Zhao, Y. Li, Cu-$Ce_{0.8}Sm_{0.2}O_{2-\delta}$ anode for electrochemical oxidation of methanol in solid oxide fuel cell: improved activity by La and Nd doping, *Solid State Ionics*, 2021, **369**, 115728, doi: 10.1016/j.ssi.2021.115728.